ACS APPLIED MATERIALS & INTERFACES

Research Article

www.acsami.org

Resistive Switching Behavior in Gelatin Thin Films for Nonvolatile Memory Application

Yu-Chi Chang and Yeong-Her Wang*

Institute of Microelectronics, Department of Electrical Engineering, and Advanced Optoelectronic Technology Center, National Cheng-Kung University, Tainan 701, Taiwan

ABSTRACT: This paper presents the characteristics of gelatin, which can cause reproducible resistive switching and bipolar resistive switching in aluminum (Al)/gelatin (35 nm)/ITO devices. The memory devices exhibited a high ON/OFF ratio of over 10^6 and a long retention time of over 10^5 seconds. The resistive switching mechanism was investigated using the high-angle dark field transmission electron microscopy image of Al/gelatin/ITO devices in the pristine high-resistance state (HRS) and then in returning to HRS after the RESET process. The energy-dispersive X-ray spectroscopy analysis revealed the aggregation of N and Al elements and the simultaneous presence of carbon and oxygen elements in the rupture of filament paths. Furthermore, via a current-sensing atomic force microscopy, we found that conduction paths in the ON-state are distributed in a highly localized area, which is associated with a carbon-rich filamentary switching mechanism. These results support that the chelation of N binding with Al ions improves the conductivity of the low-resistance state but not the production of metal filaments.

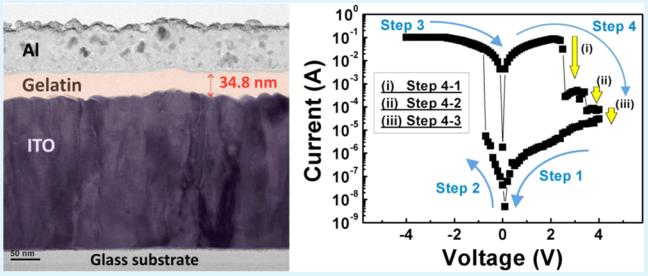

KEYWORDS: *gelatin, resistive switching, memory, chelate effect, filamentary theory*

1. INTRODUCTION

Organic materials can be produced easily and cheaply, and they have high flexibility, printing capability, easily miniaturized dimensions, and properties that can be conveniently designed through chemical synthesis. With these advantages, organic materials are suitable for low-cost resistive random access memory (RRAM) usage, can overcome the limitations of conventional silicon-based memory devices, and can increase the merits of organic-based RRAM.[1−5] Many studies have investigated functional organic materials and improved electrical memory performance in RRAM device applications.[6−8] However, crucial factors for resistive switching remain unidentified, and it is necessary to clarify the mechanism.

The electrical performance of resistive memory devices depends on the selected insulator layer. For example, various biomaterials, including enzymes,[9,10] melanin,[11] and ferritin,[12] reportedly have significant and reproducible memory-switching behavior. However, these biomaterial-based RRAM devices must be combined or stacked with other polymeric materials to enhance their performance. Moreover, these biomaterial films are unstable and difficult to store because of their sensitivity to moisture. Gelatin, which is a biomaterial, is prepared from animal collagen by heating and hydrolyzing and is suitable for a low-cost solution process because of its plasticity and excellent film formation. Studies[13] had shown that the prepared gelatin film can be stored under the atmosphere for a period of time. Moreover, the structure of gelatin is Ala-Gly-Pro-Arg-Gly-Glu-4Hyp-Gly-Pro,[14] which has a heteroatom (i.e., nitrogen or silicon) that is strongly coordinating with metal ions and an electrical conductivity that allows current to flow.[15] Thus, gelatin is potentially suitable for RRAM application.

In this study, gelatin was employed as an insulator layer, without any further purification, on ITO/glass substrate for RRAM. The electrical properties and mechanism of Al/gelatin (35 nm)/ITO RRAM were investigated. The memory devices possessed a high ON/OFF ratio of over 10^6 and a long retention time of over 10^5 seconds. We validated that the reproducible resistive switching of the Al/gelatin/ITO structure is related to the formation and rupture of the filament by directly observing the filament path within the gelatin thin film through energy-dispersive X-ray (EDX) spectroscopy mapping. Experiments by current-sensing atomic force microscopy (CS-AFM) were also conducted to visualize the distribution of local current through highly conductive paths.

2. EXPERIMENTAL SECTION

Materials and Methods. Gelatin solution was obtained from bovine skin (Sigma) and stored at 2 to 8 °C. The product specification of Type B gelatin was derived from lime-cured tissue and 2% water. The product number was G1393. ITO glass substrates (Aim Core Technology) were cut to 2.0 cm × 1.5 cm and cleaned using acetone, methanol, and deionized water in an ultrasonic bath. The gelatin solution was used without further purification, spun on the cleaned ITO substrates, and then baked in a vacuum under various temperatures. Aluminum (Al), platinum (Pt), gold (Au), and titanium

Received: September 18, 2013
Accepted: March 28, 2014
Published: March 28, 2014

   dx.doi.org/10.1021/am500815n | ACS Appl. Mater. Interfaces 2014, 6, 5413−5421

(Ti) were used as the top electrode. The top electrode area, through the shadow mask, was 0.5 mm^2. The gelatin RRAM structure is shown in the inset of Figure 1.

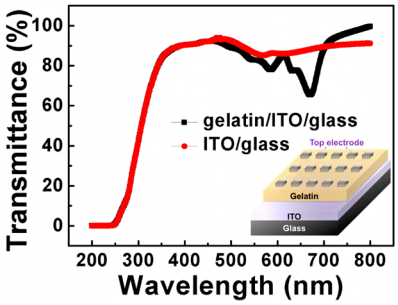

Figure 1. Transmittance spectra of ITO/glass and gelatin/ITO/glass. The inset shows the schematic illustration of the gelatin-based RRAM device.

Characterization. Samples of Al/gelatin/ITO structure were prepared for transmission electron microscopy (TEM) and scanning electron microscope (SEM) analysis. Atomic force microscopy (AFM) images were obtained using a nanoscope (Digital Instruments, USA) in tapping mode. The transmittance of the gelatin film was confirmed by ultraviolet and visible absorption spectroscopy (UV–vis) with Perkin-Elmer Lambda 35. The thermal properties of gelatin were investigated by thermogravimetric (TGA) and thermomechanical (TMA) analysis and differential scanning calorimetry (DSC) with Perkin-Elmer Pyris1, Pyris diamond thermomechanical analyzer, and TA Q500, respectively. The gelatin-based RRAM was electrically characterized using a probe station equipped with a semiconductor parameter analyzer (HP 4156B, Agilent Technologies) under atmospheric conditions at room temperature. The elements of the sample before and after measurement were mapped by EDX analysis. Samples for CS-AFM measurements were fabricated based on the gelatin/ITO structure. A Pt-coated conductive cantilever tip was used as a movable top electrode.

3. RESULTS AND DISCUSSION

Figure 1 shows that the gelatin/ITO/glass sample was transparent in the visible band. The transmittance values of gelatin/ITO/glass and ITO/glass at 550 nm were 82.78% and 86.45%, respectively. These properties render the suitability of gelatin for the fabrication of transparent electrical and optical devices.

The solvent (i.e., water) of the gelatin solution may have been within the gelatin thin film during fabrication. Thus, the effects of process parameters such as the baking temperature and time on the amount of evaporated water were investigated. The following procedures were implemented to understand the effect of surface roughness and amount of evaporated water in the gelatin thin film on the electrical performance of gelatin-based RRAM devices. First, samples T50, T80, T100, T120, and T150 were baked for 15 min and 20 h in a vacuum at 50 °C, 80 °C, 100 °C, 120 °C, and 150 °C, respectively. The morphologies of the gelatin thin films spin-coated onto the ITO glass substrates with various process parameters were confirmed by AFM, as shown in the Figure 2. R_{rms} of the gelatin thin film over the scanning area of 10 μm × 10 μm is shown in Table 1, which increased drastically under baking above 100 °C, thus indicating that the gelatin thin film was denatured by the heating temperature. The amount of evaporated water slightly decreased after being baked at various temperatures for 15 min, but rapidly decreased after being baked for 20 h, as shown in the inset of Figure 2.

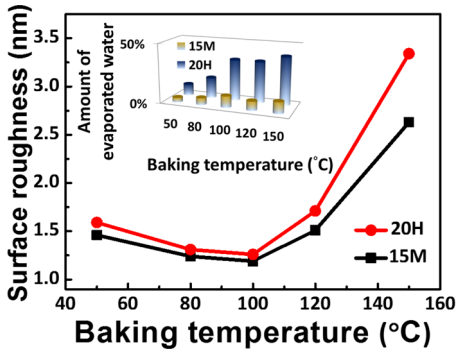

Figure 2. Surface roughness of gelatin thin films at various baking temperatures. The inset presents the relationship of evaporated water amount at various baking temperatures.

Table 1. R_{rms} of Gelatin Thin Films at Various Process Parameters

sample ID	R_{rms} [nm]	sample ID	R_{rms} [nm]
T50(15M)	1.46	**T50(20H)**	1.59
T80(15M)	1.24	**T80(20H)**	1.31
T100(15M)	1.19	**T100(20H)**	1.26
T120(15M)	1.51	**T120(20H)**	1.71
T150(15M)	2.63	**T150(20H)**	3.34

TGA, TMA, and DSC were utilized to explore the thermal properties of gelatin and subsequently investigate the trend of surface roughness. TGA is a method of investigating the thermal stability and decomposition of a material by heating. Figure 3a illustrates the TGA curves of gelatin at a heating rate of 20 °C/min under nitrogen atmosphere from 40 to 800 °C. Weight loss at temperatures below 100 °C is related to the loss of free and absorbed water. A weight loss of 3.77% was observed at 150 °C.

Four stages of decomposition were observed. The first stage of weight loss at 4% was obtained at a temperature (T_{d1}) of 159 °C. The second stage of weight loss at 8% was observed at T_{d2} of 198 °C. This stage of weight loss is due to the degradation of glycerol and the presence of small-sized protein in the film network. Hoque et al. reported that the degradation temperature for cuttlefish skin gelatin film is in the range of 196.30–216.71 °C.[16] The third stage of weight loss at 30% was observed at T_{d3} of 311 °C. This weight loss is most likely associated with the degradation of the highly associated protein fraction.[17] The fourth stage of weight loss at 43% was observed at T_{d4} of 332 °C. The thin gelatin film was baked below 150 °C ($<T_{d1}$). The gelatin exhibited stable thermal properties. Figure 3b displays the TMA thermograms of gelatin heated from 23 to 140 °C at a gradient heating rate of 20 °C/min. The softening temperature (T_s) begins at approximately 84 °C.

The DSC analysis revealed that the glass transition temperature (T_g) was 82 °C (in agreement with the T_s of 84 °C) and melting temperature (T_m) was 114 °C as shown in Figure 3c. T_g was determined from the midpoint of the change in heat flow measured during the heating temperature scan. Hence, the gelatin thin film had a slightly rough surface at a processing temperature below 82 °C. The gelatin thin film subsequently disintegrated to a carbonaceous mass with the evolution of pyridine bases and ammonia at a processing temperature above 114 °C. The roughness of the gelatin films increased as the processing temperature increased. However, at

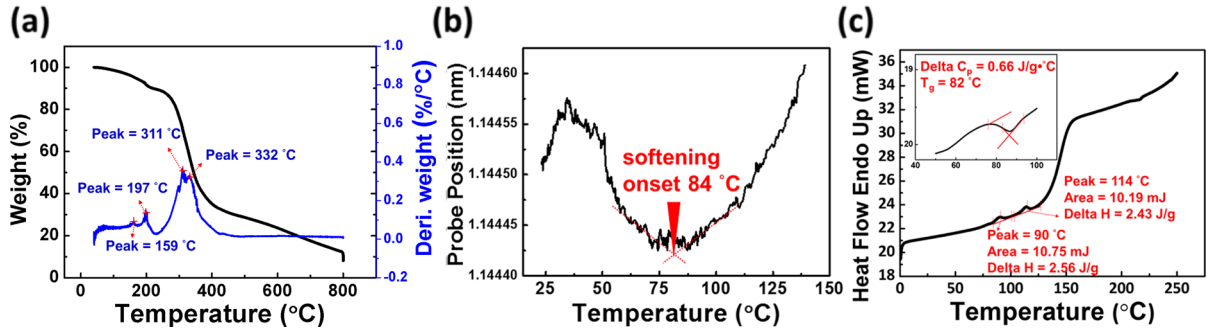

Figure 3. (a) TGA curves of gelatin. (b) TMA thermogram of gelatin measured from 23 to 140 °C. (c) DSC analysis for thermal properties of gelatin; heating temperature scans were carried out at a rate of 10 °C/min from 0 to 250 °C. The inset presents DSC thermogram measured during heating temperature scans, heating temperature scans were carried out at a rate of 20 °C/min from 50 to 100 °C.

processing temperatures below 114 °C, the surfaces of the gelatin thin films are smooth.

The ON/OFF ratio and the baking temperature as a function of process parameters are shown in Figure 4a. From these

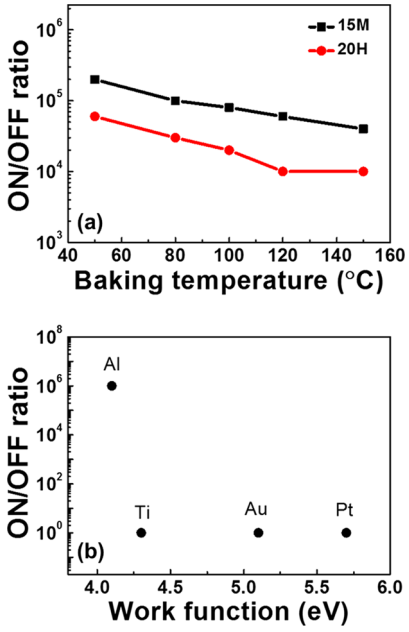

Figure 4. (a) ON/OFF ratio of gelatin-based RRAM devices at various baking temperatures. (b) ON/OFF ratio of gelatin memory device with various top electrode (i.e., Au, Al, Ti, and Pt).

results, low baking temperature is proven suitable to form the surface of gelatin thin films, while the ON/OFF ratio of gelatin-based RRAM devices is maintained at approximately 10^4 to 10^6. The metal/gelatin/ITO devices were fabricated to probe the performance of gelatin memory devices with various top electrodes (i.e., Pt, Au, Ti, and Al). The spin-coated gelatin thin films were baked in a vacuum at 50 °C for 15 min.

The ON/OFF ratios of gelatin memory devices with top electrodes of Au, Al, Pt, and Ti are shown in Figure 4b. The resistive switching behavior was observed only in the device with Al top electrode. This device had a high ON/OFF ratio of 10^6. By contrast, the memory properties were not observed clearly in devices with Pt, Au, and Ti as top electrodes.

Au (or Pt) and ITO have a high work function of more than 5 eV, whereas Al has a low work function of 4.1 eV. However, devices with Ti as the top electrode have poor memory properties despite the low work function (4.3 eV) of Ti probably because the reduced free energy of TiO_x formation is smaller than that of AlO_x. AlO_x can be formed easily between the Al top electrode and gelatin, which further enhances the performance of the device.[18] These results revealed that the switching mechanism is associated with the choice of top electrode. In addition, not only the electrode work function, but also the interface between the top electrode and gelatin film can affect the resistive switching behavior of gelatin memory devices.

Various spin-casting speeds and various thicknesses of sputtered Al were applied in fabricating devices (a) to (f) to investigate the effect of gelatin thickness and Al on the performance of gelatin memory devices. The cross-sectional images of the devices captured using SEM are shown in Table 2. Figure 5a shows that the ON/OFF ratio was around 10^5

Table 2. SEM Images of Gelatin Memory Devices

Thickness of Al/gelatin (nm)					
80/30~40	80/50~60	140/30~40	140/50~60	200/30~40	200/50~60
Device(a)	Device(b)	Device(c)	Device(d)	Device(e)	Device(f)
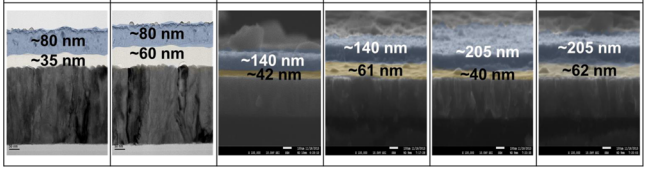					

when the thickness of the gelatin was over 50 nm and 10^6 when the thickness of the gelatin was around 30 to 40 nm. Thus, filament paths can be formed more easily at gelatin thickness of 30 to 40 nm, and the devices have better ON/OFF ratio when applied with the same voltage as that of devices (a), (c), and (e).

Moreover, Figure 5b,c reveals that devices (e) and (f) have a larger set voltage (V_{SET}) and reset voltage (V_{RESET}) than devices (a), (b), (c), and (d). The step coverage of Al consequently increased when the thickness increased to 200 nm, while the distribution of the electric field remained uniform. A large V_{SET} or V_{RESET} was therefore used to obtain a high local electric field and to form (or rupture) the filament paths.

The optimization of the experiment parameters shows that sample T50 (15M) had an excellent ON/OFF ratio and high yield. The characteristics of gelatin-based RRAM devices based on sample T50 (15M) are discussed below. Figure 6a shows a cross-sectional TEM image of an Al/gelatin/ITO resistive

dx.doi.org/10.1021/am500815n | ACS Appl. Mater. Interfaces 2014, 6, 5413−5421

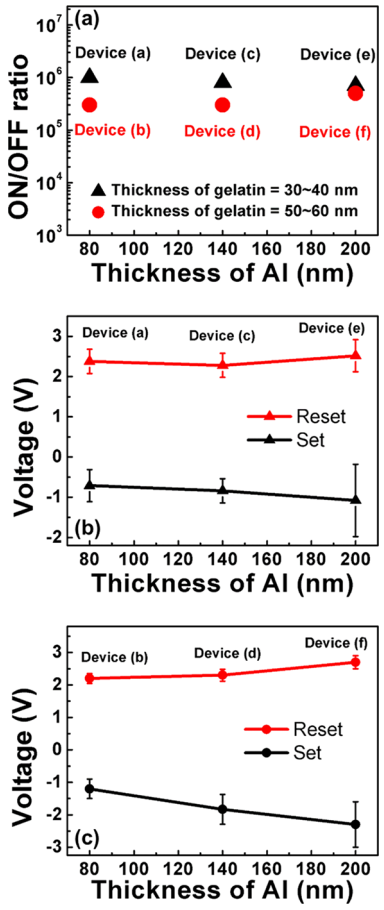

Figure 5. (a) ON/OFF ratio of gelatin memory devices with various aluminum thickness values. (b,c) Set/reset voltage of gelatin memory devices with various aluminum thickness values.

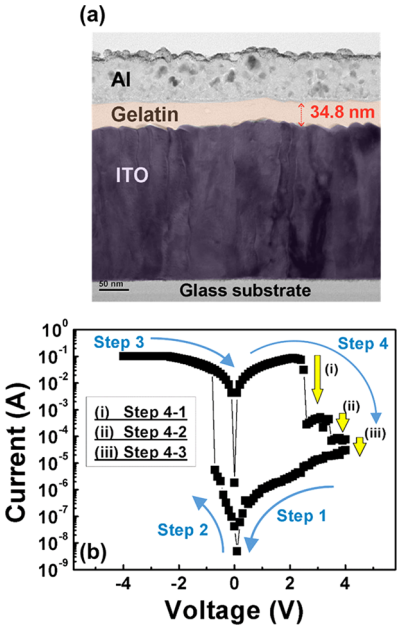

Figure 6. (a) Cross-section TEM image of the gelatin thin film fabricated on ITO/glass substrate. (b) Typical resistive switching *I*–*V* characteristics of Al/gelatin/ITO structure baked at 50 °C in a vacuum plotted on a semilogarithmic scale.

switching memory device. The thickness values of Al, gelatin, and ITO layers were 80, 35, and 260 nm, respectively. Figure 6b illustrates the characteristics of high-resolution *I*–*V*. The typical bipolar resistive switching behavior between the high-resistance state (HRS) and the low-resistance state (LRS) of the structure was observed. No electroforming process was required to turn on the devices. Moreover, +4 to −4 V was used with a limited current compliance of up to 100 mA. The arrows in Figure 6b represent the voltage sweeping direction. The device maintained HRS in the initial voltage scanned from +4 to 0 V in Step 1. A voltage sweep of 0 to −4 V was applied in Step 2, and the current increased abruptly with V_{SET} of around −0.7 V, which corresponds to the transition from HRS to LRS. The succeeding voltage sweep of −4 to 0 V was applied in Step 3, and the device remained at LRS. The final voltage sweep was 0 V to +4 V in Step 4, and the device transitioned from LRS to HRS with V_{RESET} of +2.4 V. The ON/OFF current ratio between HRS and LRS was as high as 10^6 at the reading voltage of 0.1 V. Hence, sufficient margins for sensing different resistance states were confirmed, and this application demonstrated low power consumption. Multistep RESET is frequently observed in gelatin-based memory devices, which possibly corresponds to the ruptures of multifilaments with different V_{RESET} values (as discussed below). Table 3 presents the performance comparison of the reported biomaterial-based RRAM devices.[9−12] The proposed RRAM has good ON/OFF ratio with simple fabrication process.

Table 3. Performance Comparison of Biomaterial-Based RRAMs

material	thickness [nm]	applied voltage [V]	V_{SET}/V_{RESET} [V]	ON/OFF ratio	ref
$(PAH/Ferritin)_{15}$	107	2 to −2	−1.5/1.5	~10^3	9
$(LYS/PSS)_{25}$	42	1.5 to −1.5	1/−1.3	10^2	10
$(PAH/CAT)_{15}$	52	1.8 to −1.8	−1.5/1.8	10^2	11
Melanin	--	4 to −2	−0.8/--	10^2	12
Gelatin	35	4 to −4	−0.7/2.4	~10^6	[This work]

We measured the resistance values of LRS and HRS as a function of temperature to clarify the switching mechanism of gelatin memory devices, and the result is shown in Figure 7. The resistance value of HRS decreases as the temperature increases from 300 to 400 K, and this decrease is associated with the semiconducting behavior of the thin film. By contrast,

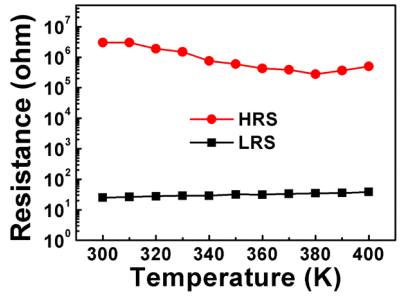

Figure 7. Resistance with various temperature variable *I*–*V* characteristics, from 300 to 400 K.

dx.doi.org/10.1021/am500815n | ACS Appl. Mater. Interfaces 2014, 6, 5413−5421

the resistance value of LRS increases as the temperature increases, indicating a weak metallic-like behavior. Thus, the resistance ratio decreases at approximately one order over a temperature range of 300 to 400 K. Ling et al. reported that if filaments were formed in a device, the ON-state current will have metallic $I-V$ characteristics and will increase as the temperature decreases.[19] Accordingly, the resistive switching behavior is related to the filament formation. In addition, the CS-AFM analysis confirmed that the resistive switching of the gelatin memory device is due to the formation and rupture of filament paths.

The formation of filament paths and the distribution of current at each state can be confirmed by CS-AFM characterization, as shown in Figure 8. The Pt-coated conductive

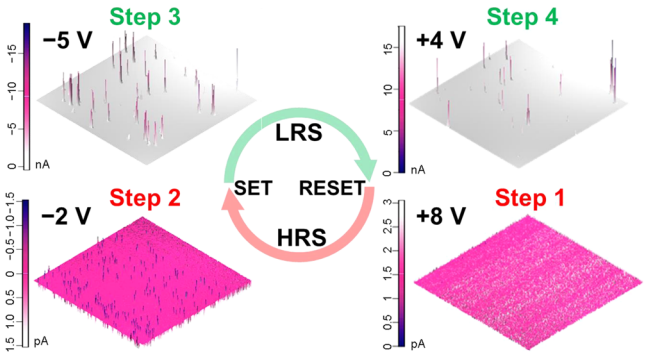

Figure 8. CS-AFM images of gelatin film in the ON and OFF states during the set and reset voltage sweep. CS-AFM images were measured with an electrochemically inert platinum top electrode, instead of an aluminum electrode.

cantilever as a movable top electrode was scanned over an area of 10 μm × 10 μm in the CS-AFM experiment. The current was very low throughout the entire scanned region, with the positive voltage sweep of 0 V to +8.0 V in Step 1 indicating HRS. At −5.0 V in Step 3, the device switched from OFF (low-conductance state) to ON (high-conductance state), and filament paths formed. The ON state was maintained in the voltage sweep of −5.0 V to +4.0 V, as shown in Step 4. Finally, the filament paths were broken down, switching the device from ON to OFF state. The formation and rupture of the filament paths were observed after the SET and RESET processes, indicating that the current density between the top and bottom electrodes was not uniform, which resulted in the increase in the applied voltage to a value higher than that of the $I-V$ characteristics (−0.7 and 2.4 V). These phenomena arose because Al electrodes (area of 0.5 mm^2) were utilized as the top electrode for the measurement of the gelatin memory device (Figure 6b). In Figure 8, the Al electrodes are replaced by a conducting AFM tip electrode (electrical point source with an additionally small contact area of approximately 30 nm), resulting in the increase in resistance. The additional energy barrier between the gelatin film and the conducting AFM tip electrode caused low conductivity. Therefore, relatively higher operation voltage and lower conductivity are exhibited in the CS-AFM data (Figure 8) than in the $I-V$ curve (Figure 6b). In addition, this current density was concentrated in the filament paths, which switched the device from ON to OFF state.

The filamentary theory has reported two types of filamentary conduction. The first type is related to the formation of carbon-rich filaments, while the second type is related to metallic filaments formed by the migration or sputtering of electrodes through films.[20−22] Thus, the formation and rupture of filaments and the composition of Al/gelatin/ITO structures can be analyzed by EDX.

Figure 9a,b presents the EDX images of the Al/gelatin/ITO structure in the pristine HRS, with no voltage applied and after the RESET process, respectively. The distribution trends of several elements (i.e., N, O, C, Al, In, and Sn) can be classified into three parts.

Migration of Metal Ions. Al, indium (In), and tin (Sn) atoms were observed in the gelatin thin film after the reproducible resistive switching as a result of voltage application, and several Al atoms were stacked at the interface between the gelatin thin film and the bottom electrode (ITO) because of chemical oxidation (eq 1) and chemical redox reaction (eq 2). In addition, the aluminum oxide layer (Al_2O_3) between the Al top electrode and the gelatin thin film acted as a barrier that prevented the migration of In and Sn ions.[23] As a result, the In and Sn atoms were not distributed because some of these atoms were stacked at the interface between the gelatin thin film and the Al_2O_3 layer.

$$Al \rightarrow Al^{3+} + e^- \quad (1)$$

$$Al^{3+} + e^- \rightarrow Al \quad (2)$$

Aggregation of Nitrogen (N) and Al. The aggregation and effect of N atoms in the gelatin thin film were thoroughly investigated. The typical amino acid sequence of gelatin is Ala-Gly-Pro-Arg-Gly-Glu-4Hyp-Gly-Pro.[24] Figure 10a illustrates the gelatin structure when controlled by temperature. The α-helical structure of the gelatin strands can melt by increasing the temperature, while many polypeptide chains are in a random coil conformation that contains both positive and negative charges.[25] During baking, negatively charged ions were generated by the interaction of water molecules with hydroxyl in amino groups in the gelatin. The glutamic acid of gelatin bound with metal ions (Al^{3+}), and then the chelate effect occurred. Figure 10b presents the chemical structure of glutamic acid, and Figure 10c illustrates that Al−N and Al−O bonds can be formed by applying voltage. All biochemical substances displayed the ability to dissolve certain metal cations, such as histidine, glutamic acid, malate, and polypeptides, which are called chelators.[26] Chelation in the gelatin thin film occurred after voltage was applied. However, the effect of chelation on memory properties remains to be clarified.

Formation of Carbon-Rich Filament Path. The gelatin micelles contain positive and negative charges which may have effects on the switching behavior. As the results shown above, the switching behavior is very similar to that of the MIM RRAM structure. The gelatin is an insulator after baking and the total charge is zero. It can then be treated as the insulator in the MIM RRAM. The filament path may play an important role in carrier transport.

Figure 9b shows that carbon was mainly detected in the gelatin thin film. No metallic filament path can be observed between the top and bottom electrodes, but with the rupture of the filament paths characterized by carbon and oxygen, the carbon-rich filamentary conducting paths contributed to the high current flow in the ON state. Thus, we suggest that the distribution of element C and O might be the rupture of the filament path.

dx.doi.org/10.1021/am500815n | ACS Appl. Mater. Interfaces 2014, 6, 5413−5421

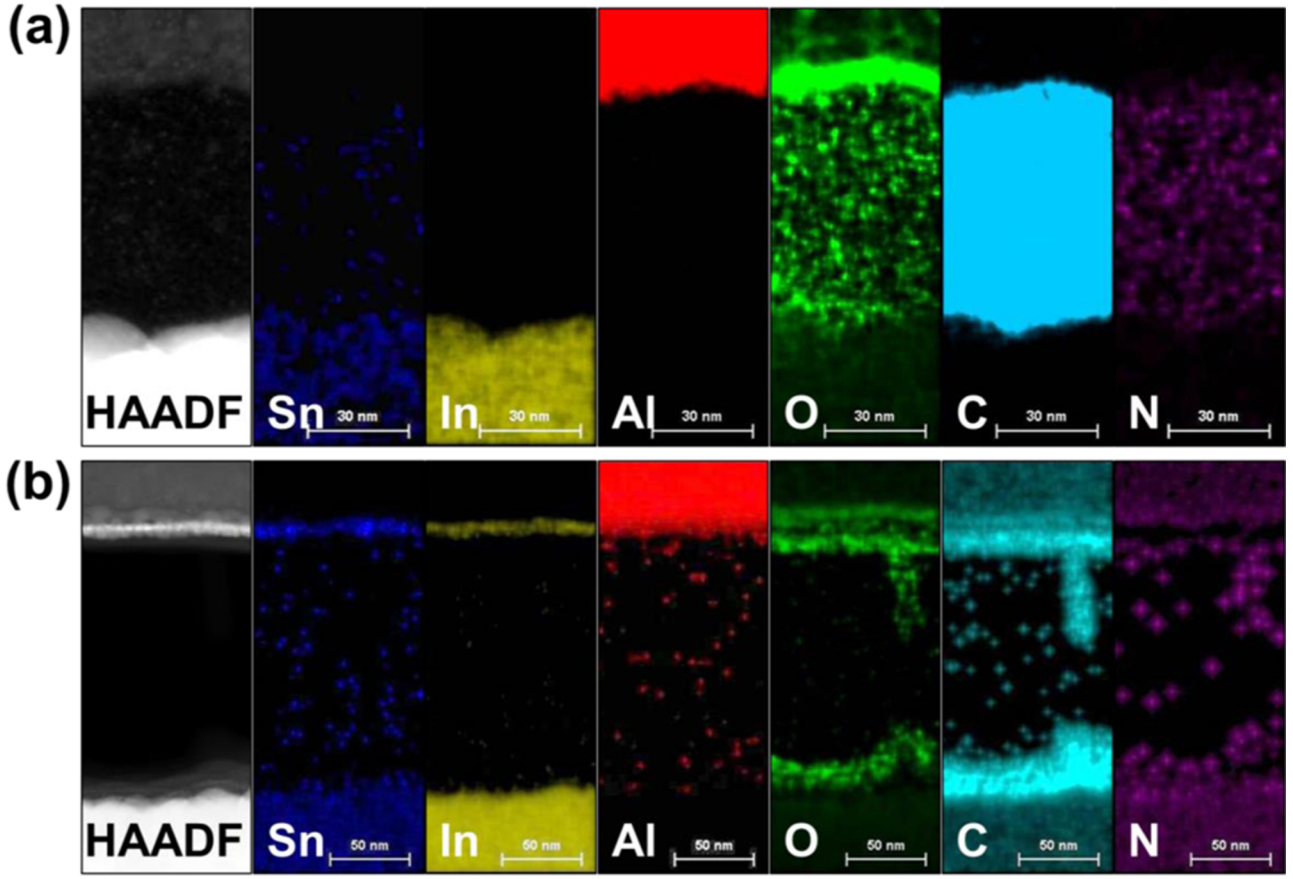

Figure 9. High-angle dark field image of Al/gelatin/ITO memory (a) in the pristine HRS without applied voltage and (b) returning to the HRS after the RESET; Sn, In, Al, O, C, and N were mapped by EDX analysis.

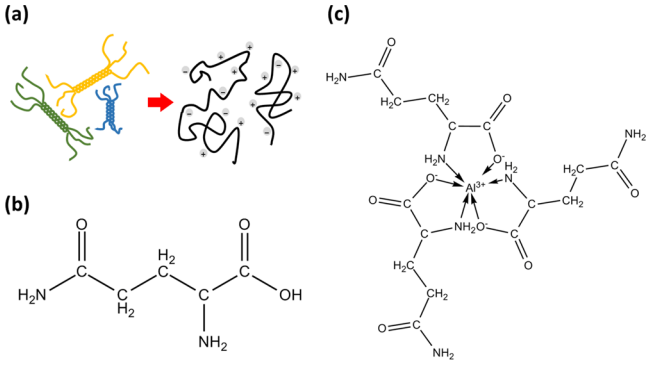

Figure 10. (a) α-Helical structure of gelatin strands can be melted by increasing the temperature and can reversibly reconstitute upon cooling, with α-helices interacting to induce the chelation of the solution. (b) Chemical structure of glutamine. (c) Chemical structure of Al-chelation.

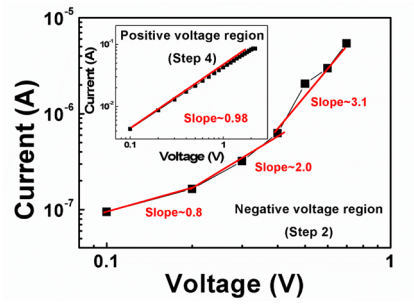

Figure 11. Linear fitting for the $I-V$ curve of a gelatin-based memory device plotted on a log–log scale during the SET process in a negative voltage sweep and during the RESET process in a positive sweep. The red lines show the fitting results.

To further clarify on the conduction mechanisms of the gelatin-based RRAM device, the obtained typical $I-V$ characteristics were investigated, as shown in Figure 11. The $I-V$ relationship in the high-conductance state (ON state) exhibited ohmic conduction behavior with a slope of around 0.98, indicating the formation of filament paths in the device during the SET process. By contrast, the fitting result in the low-conductance state (OFF state) indicated that the charge transport behavior is consistent with the trap-controlled space charge limited conduction (SCLC) model.[27,28] The SCLC model describes the following three different conductive regions: (1) a low-voltage region where the $I-V$ curve exhibits linear behavior with a slope of around 0.8 ($I \propto V$), which corresponds to the ohmic conduction mechanism, (2) a transition region where the current increases nonlinearly with voltage square dependence ($I \propto V^2$) and the slope increases to 2.0, which is close to the Child's law, and (3) a region marked by a sharp increase in current where the slope is around 3.2. The results of the investigation on the $I-V$ characteristics reveal that the different conduction behaviors of the gelatin-based RRAM device are governed by SCLC and the formation of localized filament paths.

The noncomplete RESET (Figure 12a) and multistep RESET (Figure 4) processes were frequently observed in the $I-V$ curves of the gelatin-based RRAM devices. These

dx.doi.org/10.1021/am500815n | ACS Appl. Mater. Interfaces 2014, 6, 5413–5421

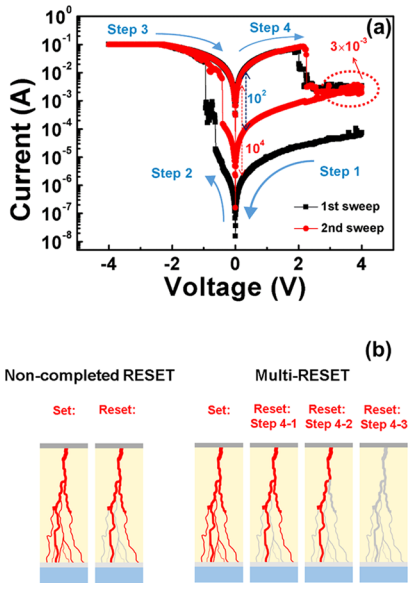

Figure 12. (a) *I*–*V* curve of the noncomplete RESET process. (b) Procedures of filament paths rupturing under noncomplete RESET and multi-RESET conditions.

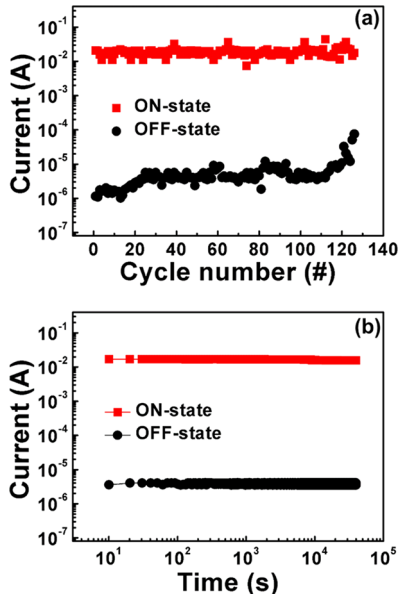

Figure 13. (a) Endurance performance at reading voltage of 0.5 V. (b) Retention test for ON and OFF states.

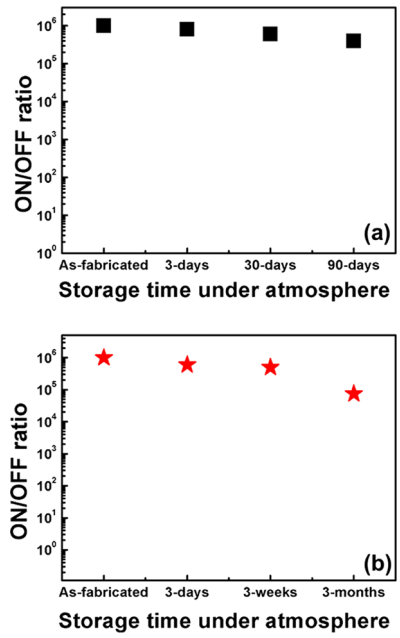

Figure 14. ON/OFF ratio as a function of storage time for (a) gelatin thin films and (b) gelatin memory devices under atmosphere conditions.

phenomena may be consistent with the partial rupture of multifilament paths at different V_{RESET} (Figure 12b). Fresh weak filaments may gather to form more stable and wider filaments because of the increased number of sweeps. These formed filaments then result in filament paths of different shapes in the gelatin thin film, indicating that the RESET process has to be applied at different V_{RESET} to rupture all filaments. In addition, during the noncomplete RESET process, Step 1 of the second sweep starts at high current and reduces the ON/OFF ratio of the gelatin-based RRAM. Therefore, if gelatin-based RRAM devices can rupture multifilaments completely during the multistep RESET process, the start current of the sweep in Step 1 in HRS will be lowered, and the ON/OFF ratio of the gelatin-based RRAM will be enhanced.

Figure 13a presents the reproducibility achieved at a voltage reading of 0.5 V for the gelatin-based memory device. The switching cycles can be repeated over 120 cycles. Figure 13b illustrates the retention ability at the voltage reading of 0.5 V per 100 s to further investigate stability. The current in the ON and OFF states was obtained after each state was switched. The resistance ratio remained higher than 10^3 without disturbance for over 10^5 seconds at room temperature, signifying the nondestructive readout properties and the nonvolatile nature of the gelatin-based memory device.

The hydrophilic properties of the gelatin material affected the performance of the gelatin memory devices. Thus, we designed two experiments. First, the gelatin/ITO/glass samples were placed under atmospheric environment (room temperature: 22 to 28 °C and relative humidity: 70% to 88%) for 3, 30, and 90 days, respectively. The samples were then sputtered with Al as top electrode to fabricate the gelatin memory devices. The experiment results are shown in Figure 14a. The second experiment involved gelatin memory devices placed under atmospheric environment (room temperature: 22 to 28 °C and relative humidity: 70% to 88%). After 3, 30, and 90 days, these devices were measured. The experiment results are shown in Figure 14b. Figure 14a,b shows that when the gelatin thin films were placed under atmospheric environment for 90 days, the gelatin memory devices retained good ON/OFF ratio of around 10^6. Meanwhile, the gelatin devices that were placed under atmospheric environment for 30 days had the same result. The gelatin memory devices placed under atmospheric environment for more than 90 days had an ON/OFF ratio of approximately 10^5. The conductivity of these devices also decreased and flaked off easily. The results proved that good electrical performance of the gelatin memory devices can be achieved by employing appropriate manufacturing techniques.

4. CONCLUSIONS

This paper presents the bipolar resistive switching behavior of the Al/gelatin/ITO sandwich structure. The simple-processed

dx.doi.org/10.1021/am500815n | ACS Appl. Mater. Interfaces 2014, 6, 5413–5421

gelatin RRAM can achieve a higher ON/OFF current ratio than 10^6 and retention time of over 10^5 seconds. The migration of metal ions and the aggregation of several elements in the gelatin thin film were confirmed by EDX analyses. Both π-conjugation and coordinating atoms (i.e., N atoms) that can be bound to metal ions are found generally essential in producing filaments. These results further support that the chelation of N bound with Al ions improves the conductivity of LRS, but not the production of metal filaments. The resistive switching mechanism of the gelatin-based RRAM was investigated based on the fitting results (or SCLC model) of electrical measurements, and CS-AFM analysis remained consistent with the formation and rupture of filaments. Carbon-rich objects were identified as factors in forming conductive filaments, which maintain the ON current state. Moreover, multifilament paths can be ruptured completely by multistep RESET. The low starting current in HRS can be achieved, thus improving the ON/OFF ratio of the gelatin-based RRAM. These results provide insight into the resistive switching mechanism in gelatin-based RRAM and the possibility of enhancing memory performance.

AUTHOR INFORMATION

Corresponding Author

*E-mail: yhw@ee.ncku.edu.tw.

Notes

The authors declare no competing financial interest.

ACKNOWLEDGMENTS

This work was supported in part by the National Science Council of Taiwan under contracts NSC99-2627-E-006-003, NSC98-2221-E-006-213-MY3, NSC NSC101-2221-E-006-141-MY3, and NSC102-222-E-006-182-MY3. We also thank Dr. Yong-Fen Hsieh, Dr. Chung-Ho Kao, Mr. Fox Yeh, and Miss Ying-Huei Lin (MA-tek) for sample preparation and TEM observation.

ABBREVIATIONS

RRAM, resistive random access memory; EDX, energy-dispersive X-ray spectroscopy; CS-AFM, current-sensing atomic force microscopy; UV−vis, ultraviolet and visible absorption spectroscopy; TEM, transmission electron microscopy; TGA, thermogravimetric analysis; TMA, thermomechanical analysis; DSC, differential scanning calorimetry; HRS, high-resistance state; LRS, low-resistance state; SCLC, space charge limited conduction; PAH, poly-(allylamine hydrochloride); LYS, lysozyme; PSS, poly(styrene sulfonate); CAT, catalase

REFERENCES

(1) Ma, D.; Aguiar, M.; Freire, J. A.; Huemmelgen, I. A. Organic Reversible Switching Devices for Memory Applications. *Adv. Mater.* **2000**, *12*, 1063−1066.

(2) Moller, S.; Perlov, C.; Jackson, W.; Taussig, C.; Forrest, S. R. A Polymer/Semiconductor Write-Once Read-Many-Times Memory. *Nature* **2003**, *426*, 166−169.

(3) Ling, Q.; Song, Y.; Ding, S. J.; Zhu, C.; Chan, D. S. H.; Kwong, D. L.; Kang, E. T.; Neoh, K. G. Non-Volatile Polymer Memory Device Based on a Novel Copolymer of N-Vinylcarbazole and Eu-Complexed Vinylbenzoate. *Adv. Mater.* **2005**, *17*, 455−459.

(4) Sekitani, T.; Someya, T. Stretchable, Large-Area Organic Electronics. *Adv. Mater.* **2010**, *22*, 2228−2246.

(5) Chu, C. W.; Ouyang, J.; Tseng, J. H.; Yang, Y. Organic Donor−Acceptor System Exhibiting Electrical Bistability for Use in Memory Devices. *Adv. Mater.* **2005**, *17*, 1440−1443.

(6) Zhuang, X. D.; Chen, Y.; Liu, G.; Zhang, B.; Neoh, K. G.; Kang, E. T.; Zhu, C. X.; Li, Y. X.; Niu, L. J. Preparation and Memory Performance of a Nanoaggregated Dispersed Red 1-Functionalized Poly (N -vinylcarbazole) Film via Solution-Phase Self-Assembly. *Adv. Funct. Mater.* **2010**, *20*, 2916−2922.

(7) Teo, E. Y. H.; Ling, Q. D.; Song, Y.; Tan, Y. P.; Wang, W.; Kang, E. T.; Chan, D. S. H.; Zhu, C. Non-Volatile WORM Memory Device Based on an Acrylate Polymer with Electron Donating Carbazole Pendant Groups. *Org. Electron.* **2006**, *7*, 173−180.

(8) Kondo, T.; Lee, S. M.; Malicki, M.; Domercq, B.; Marder, S. R.; Kippelen, B. A Nonvolatile Organic Memory Device Using ITO Surfaces Modified by Ag-Nanodots. *Adv. Funct. Mater.* **2008**, *18*, 1112−1118.

(9) Baek, H.; Lee, C.; Lim, K.; Cho, J. Resistive Switching Memory Properties of Layer-by-Layer Assembled Enzyme Multilayers. *Nanotechnology* **2012**, *23*, 155604−9.

(10) Baek, H.; Lee, C.; Lim, K.; Park, J.; Kim, Y.; Koo, B.; Shin, H.; Wang, D.; Cho, J. Layer-by-Layer Assembled Enzyme Multilayers with Adjustable Memory Performance and Low Power Consumption via Molecular-Level Control. *J. Mater. Chem.* **2012**, *22*, 4645−4651.

(11) Ko, Y.; Kim, Y.; Baek, H.; Cho, J. Electrically Bistable Properties of Layer-by-Layer Assembled Multilayers Based on Protein Nanoparticles. *ACS Nano* **2011**, *5*, 9918−9926.

(12) Ambrico, M.; Cardone, A.; Ligonzo, T.; Augelli, V.; Ambrico, P. F.; Cicco, S.; Farinola, G. M.; Filannino, M.; Perna, G.; Capozzi, V. Hysteresis-Type Current−Voltage Characteristics in Au/Eumelanin/ITO/Glass Structure: Towards Melanin Based Memory Devices. *Org. Electron.* **2010**, *11*, 1809−1814.

(13) Schmitz, N. *Haltbarkeit photographischer Schichten*; Berichte Der Internationaler Kongress Fuer Reprographie: Germany, 1963; pp 74−76.

(14) Tungkavet, T.; Pattavarakorn, D.; Sirivat, A. Bio-Compatible Gelatins (Ala-Gly-Pro-Arg-Gly-Glu-4Hyp- Gly-Pro-) and Electromechanical Properties: Effects of Temperature and Electric Field. *J. Polym. Res.* **2012**, *19*, 9759−9.

(15) Joo, W. J.; Choi, T. L.; Lee, J.; Lee, S. K.; Jung, M. S.; Kim, N. J.; Kim, M. Metal Filament Growth in Electrically Conductive Polymers for Nonvolatile Memory Application. *J. Phys. Chem. B* **2006**, *110*, 23812−23816.

(16) Hoque, M. S.; Benjakul, S.; Prodpran, T. Properties of Film from Cuttlefish (Sepia pharaonis) Skin Gelatin Incorporated with Cinnamon, Clove and Star Anise Extracts. *Food Hydrocolloids* **2011**, *25*, 1085−1097.

(17) Tongnuanchan, P.; Benjakul, S.; Prodpran, T. J. Physico-Chemical Properties, Morphology and Antioxidant Activity of Film from Fish Skin Gelatin Incorporated with Root Essential Oils. *Food Eng.* **2013**, *117*, 350−360.

(18) Verbakel, F.; Meskers, C. J.; Janssen, R. A. J.; Gomes, H. L.; Cölle, M.; Büchel, M.; Leeuw, D. M. Reproducible Resistive Switching in Nonvolatile Organic Memories. *Appl. Phys. Lett.* **2007**, *91*, 192103−3.

(19) Ling, Q. D.; Liaw, D. J.; Zhu, C.; Chan, D. S. H.; Kang, E. T.; Neoh, K. G. Polymer Electronic Memories: Materials, Devices and Mechanisms. *Prog. Polym. Sci.* **2008**, *33*, 917−978.

(20) Ji, Y.; Choe, M.; Cho, B.; Song, S.; Yoon, J.; Ko, H. C.; Lee, T. Organic Nonvolatile Memory Devices with Charge Trapping Multilayer Graphene Film. *Nanotechnology* **2012**, *23*, 105202−6.

(21) Segui, Y.; Ai, B.; Carchano, H. Switching in Polystyrene Films: Transition from On to Off State. *J. Appl. Phys.* **1976**, *47*, 140−143.

(22) Hwang, W.; Kao, K. C. On the Theory of Filamentary Double Injection and Electroluminescence in Molecular Crystals. *J. Chem. Phys.* **1974**, *60*, 3845−11.

(23) Ju, Y. C.; Kim, S.; Seong, T. G.; Nahm, S.; Chung, H.; Hong, K.; Kim, W. Resistance Random Access Memory Based on a Thin Film of CdS Nanocrystals Prepared via Colloidal Synthesis. *Small* **2012**, *8*, 2849−2855.

(24) Oh, J. K.; Lee, D. I.; Park, J. M. Biopolymer-Based Microgels/Nanogels for Drug Delivery Applications. *Prog. Polym. Sci.* **2009**, *34*, 1261−1282.
(25) Mezzenga, R.; Fischer, P. The Self-Assembly, Aggregation and Phase Transitions of Food Protein Systems in One, Two and Three Dimensions. *Rep. Prog. Phys.* **2013**, *76*, 046601−43.
(26) Lippard, S.; Berg, J. J. M. *Principles of Bioinorganic Chemistry*; University Science Books: Mill Valley, CA, 1994.
(27) Kim, Y.; Lee, C.; Shim, I.; Wang, D.; Cho, J. Nucleophilic Substitution Reaction Based Layer-by-Layer Growth of Superparamagnetic Nanocomposite Films with High Nonvolatile Memory Performance. *Adv. Mater.* **2010**, *22*, 5140−5144.
(28) Yang, Y. C.; Pan, F.; Liu, Q.; Liu, M.; Zeng, F. Fully Room-Temperature-Fabricated Nonvolatile Resistive Memory for Ultrafast and High-Density Memory Application. *Nano Lett.* **2009**, *9*, 1636−1643.